Physica Medica 85 (2021) 87–97

Contents lists available at ScienceDirect

Physica Medica

journal homepage: www.elsevier.com/locate/ejmp

Original paper

An interictal measurement of cerebral oxygen extraction fraction in MRI-negative refractory epilepsy using quantitative susceptibility mapping

Tayyebeh Ebrahimi [a,b], Abbas Tafakhori, associate professor [c], Hassan Hashemi [d], Mohammad Ali Oghabian [a,b,e,*]

[a] Department of Medical Physics and Biomedical Engineering, School of Medicine, Tehran University of Medical Sciences, Tehran, Iran
[b] Department of Neuroimaging and Analysis, Imam Khomeini Hospital Complex, Tehran University of Medical Sciences, Tehran, Iran
[c] Iranian Center of Neurological Research (ICNR), Neuroscience Institute, Tehran University of Medical Sciences, Tehran, Iran
[d] Advanced Diagnostic and Interventional Radiology Research Center (ADIR), Tehran University of Medical Sciences, Tehran, Iran
[e] Research Center for Molecular and Cellular Imaging, Tehran University of Medical Science, Tehran, Iran

ARTICLE INFO

Keywords:
MRI-negative refractory epilepsy
Oxygen extraction fraction
Quantitative susceptibility mapping
Hypometabolism

ABSTRACT

Purpose: Oxygen extraction fraction (OEF) can be a factor to identify brain tissue's disability in epileptic patients. This study aimed to assess the OEF's level measurement in refractory epileptic patients (REPs) using a quantitative susceptibility mapping (QSM) method and to determine whether the OEF parameters change.
Methods: QSM-OEF maps of 26 REPs and 16 healthy subjects were acquired using 3T MRI with a 64-channel coil. Eighteen regions-of-interest (ROIs) were chosen around the cortex in one appropriate slice of the brain and the mean QSM-OEF for each ROI was obtained. The correlations of QSM-OEF among different clinical characteristics of the disease, as well as between the patients and normal subjects, were also investigated.
Results: QSM-OEF was shown to be significantly higher in REPs (44.9 ± 5.8) than that in HS (41.9 ± 6.2) ($p < 0.05$). Mean QSM-OEF was statistically lower in the ipsilateral side (44.5 ± 6.6) compared to the contralateral side (46.4 ± 6.8) ($P < 0.01$). QSM-OEF was illustrated to have a strong positive correlation with the attack duration ($r = 0.6$), and a moderate negative correlation with the attack frequency ($r = -0.3$). Using an optimized support vector machine algorithm, we could predict the disease in subjects having abnormal OEF values in the brain-selected-ROIs with sensitivity, specificity, AUC, and the precision of 0.96, 1, 0.98, and 1, respectively.
Conclusions: The results of this study revealed that QSM-OEF of the REPs' brain is higher than that of HS, which indicates that QSM-OEF is associated with disease activity.

1. Introduction

Epilepsy is defined to be seized or attacked and arises from disorders related to the central nervous system as well as disturbed nerve cell function [1]. According to WHO statistics in 2018, nearly 65 million people in the world suffer from epilepsy [2]. At least two motiveless seizures are required for the epilepsy diagnosis. Several factors, such as head injuries, hypoxia during birth, brain tumors, and infections, lead to symptomatic epilepsies [3]. Hippocampal sclerosis is the most prevalent pathological magnetic resonance imaging (MRI) finding among refractory epileptic patients (REPs) candidates for anterior temporal lobectomy. Other pathological MRI findings include focal cortical dysplasia (FCD), vascular malformations, and post-infection. However, a significant epileptic population involves normal MRI findings that complicate recognizing the epileptogenic zone [4]. Therefore, other methods than conventional MRI analysis are required to assess brain changes in epileptic patients. Vikram et al. [5] have reviewed the state-of-the-art progressions in assortment algorithms to find seizure phases, seizure sensing, signal processing, and frequency-domain analysis, as well as the essentials for brain stimulation methods. To describe the status of oxygen alterations at the veins, knowing the two prime factors is necessary: oxygen supply (depending on hemoglobin accessibility) and oxygen extraction fraction (OEF) (which depends mainly on the metabolic rate of the neurons [6]).

OEF is defined as the ratio of the oxygen supplied through blood flow and the oxygen demand of brain tissue, a high function of physiological

* Corresponding author at: Department of Medical Physics and Biomedical Engineering, School of Medicine, Tehran University of Medical Sciences, Tehran, Iran.
E-mail addresses: t_ebrahimi@razi.tums.ac.ir (T. Ebrahimi), a_tafakhori@sina.tums.ac.ir (A. Tafakhori), hashemi_mic@yahoo.com (H. Hashemi), oghabian@sina.tums.ac.ir (M. Ali Oghabian).

https://doi.org/10.1016/j.ejmp.2021.03.039
Received 8 January 2021; Received in revised form 19 March 2021; Accepted 30 March 2021
Available online 10 May 2021

factors [7]. Although the relationships between oxygen metabolism and seizure patterns have not been well established, intense neuronal firing during epileptic seizures followed by enhanced energy consumption has been studied by electrophysiological recordings [8]. Farrell et al. [9] measured the local brain tissue oxygenation levels in rodents. The hippocampal PO_2 levels altered between 18 and 30 mm Hg (termed normoxia range) during normal behaviors. However, after succinct neuronal stimulations, local PO_2 levels decreased below 10 mm Hg, in which the severity of hypoxia was positively correlated with stimulation duration and cerebral blood flow (CBF). It is noteworthy that PO_2 values of less than 10 mm Hg are considered as severely hypoxic and are associated with the induction of hypoxia-dependent gene expression [10].

The relationship between deficiencies in cerebral blood supply and the oxygen metabolism is termed misery perfusion [11], which raises the probability of stroke recurrence in patients who have major cerebral arterial occlusive symptoms [12]. Anatomic studies following frequent seizures have shown several alterations, including enhanced blood–brain barrier (BBB) permeability [13], the formation of new capillaries [14], central inflammation [15], and neuronal loss [16]. Regarding the aforementioned studies, we hypothesized that the disease activity related to capillary problems and hypometabolism could increase the OEF in the REPs when the amount of reduction in cerebral blood flow (CBF) is more severe than the decrease of cerebral metabolic rate of oxygen ($CMRO_2$). Although positron emission tomography (PET) has been introduced as the gold standard method for OEF measurements, there are several reasons, such as high expenses, limited accessibility, and radiation exposure [17] which prevent PET to become a standard clinical diagnosis tool for imaging abnormal cerebral oxygen metabolism in patients. To date, a few developed MRI-based approaches for OEF measurement [18–20] have been applied to clinical cohorts.

Quantitative susceptibility mapping (QSM) is a newfound post-processing technique that employs phase images to measure the magnetic susceptibility of various tissues [21]. The shape and orientation of veins related to the main field, as well as dipolar artifacts, affect the measured distribution of phase values. Since QSM is insensitive to these factors, we can measure OEF's absolute quantity through susceptibility of deoxyhemoglobin [dHb] in venous only through once data acquisition. Hence, an oxygen-based contrast can be provided through susceptibility maps without injection [22]. Uwano et al. [23] and Nomura et al. [24] demonstrated a good correlation between OEF measurements using the QSM of 7 T MRI and the gold standard ^{15}O PET in the identification of elevated OEF in affected hemispheres of patients with chronic ischemia. In another study, Kakeda et al. [25] reported the increment of QSM-OEF in the systemic lupus erythematosus (SLE) patients which might predict an increased risk of stroke in SLE.

The purposes of this study were to evaluate the QSM-OEF variations in REPs and determine whether QSM-OEF is associated with the disease characteristic in epileptic patients.

2. Methods

2.1. Subjects

From October 2018 to February 2020, out of all epileptic patients admitted to the Epilepsy Clinic of Imam Khomeini Hospital (Tehran, Iran), 26 MRI-negative REPs were selected based on ILAE definition that specified as a failure of adequate trials of two tolerated and appropriately chosen anti-epileptic drugs [26]. These subjects included 14 females and 12 males with ages ranging from 15 to 56 years (mean ± SD; 29.31 ± 8.86). Seventeen patients had focal-onset, and the rest had generalized-onset seizures. Two blinded radiologists did not recognize any lesions in the patient's conventional MRI images, including T1-MPRAGE (3D), T2-FLAIR, and T2W-FSE images. The semiology data of the patients are demonstrated in Table 1. Furthermore, 16 age-matched subjects, including 9 females and 7 males, with ages ranging from 22 to 59 years (mean ± SD of 31.13 ± 8.45), were enrolled as healthy subjects (HS). All HS had normal MR images without any clinical history of CNS diseases, alcohol abuse, severe head trauma, or febrile seizures. Written informed consent was obtained from all participants to take part in the study. The experiment protocol was approved by the Local Ethics Committee of the Tehran University of Medical Sciences (TUMS).

Table 1
Clinical information of the non-lesional refractory epileptic patients (REPs).

No.	Sex	Age (yrs)	Age-onset (yrs)	Frequency (month)	Duration of attack (min)	Seizure before MRI (day)	LTM finding
1	F	26	5	2	5	50	RT mesial temporal
2	F	48	2	20	1	2	LT mesial temporal
3	M	25	1	25	5	1	Bilateral frontal
4	M	24	13	60	3	1	LT mesial temporal
5	M	25	16	3	10	23	LT temporal focal
6	F	34	7	2	2	1	RT mesial temporal
7	F	26	10	2	0.16	10	LT fronto- central
8	F	34	22	3	10	15	GME
9	M	16	12	2	2	22	RT mesial frontal
10	M	28	24	1	2	20	RT frontal
11	F	34	5	10	7	1	GME
12	M	37	7	1	7	20	RT temporal
13	M	31	15	3	3	1	RT temporal
14	M	17	12	2	1	1	LT fronto- central
15	M	30	9	30	5	0.8	LT frontal
16	F	43	35	9	2	2	RT frontal focal
17	F	24	5	30	0.16	0.5	LT frontal focal
18	F	31	7	2	0.19	30	RT fronto- temporal
19	M	21	1	1	10	20	RT frontal focal
20	F	50	17	3	3	20	GME
21	F	15	10	0.3	5	30	GTC
22	F	27	13	1	5	20	GME
23	F	27	13	2	10	60	JME
24	F	21	16	0.2	15	60	GTC
25	M	34	14	10	6	0.1	GME
26	M	30	16	0.5	5	30	GTC

RT = right, LT = left, M = male; F = female, LTM = long time monitoring, GTC = generalized tonic-clonic, GME = Generalized myoclonic epilepsy, JME = juvenile myoclonic epilepsy

2.2. MRI acquisition

All images were taken using a 3.0 T Siemens whole-body scanner (Prisma, Healthcare, Germany) with a high-resolution standard transmit/receive 64 channel head/neck coil. Data acquisition was performed using a whole-brain 3D SPGR sequence with four echoes. A major factor in selecting TE is the susceptibility of dHb. At longer TEs, phase SNR is higher, while shorter TEs lead to less phase wrapping [21,27]. Therefore, TE of 14 ms was considered to have less phase wrapping between the vessels and background tissue in a 3 T scanner. The scan parameters included: first TE = 14 ms, ΔTE = 7 ms, TR = 41 ms, pixel size = 0.625 × 0.625 mm^2, acquisition matrix = 384 × 268 × 60, reconstruction matrix = 384 × 384 × 60, slice thickness = 2 mm, FA = 15°, and GRAPPA factor = 2. The level of the cerebellum to the high convexity was set for the imaging slab. T1-MPRAGE and T2W- FSE were taken as anatomical images.

2.3. Post-processing of OEF

To reduce the effects of blood flow inside the veins and less signal omission, the first echo in which flow compensation is applied in three directions was used to create the OEF map. QSM images were generated using the STI-Suite toolbox [28,29] in which phases are derived from imaginary and real images to measure the magnetic field inhomogeneity, which is subsequently inverted to assess the infrastructural susceptibility distribution. The STI-Suite approach uses the Laplacian method to phase unwrapping, the variable kernel sophisticated harmonic artifact reduction for phase (V-SHARP) to background removal, and iterative least-squares regression (iLSQR) to reconstruct QSM. The magnetic susceptibilities were referenced to the average susceptibility of the brain (0 ppm). In this work, the upper thirty QSM images from sixty slices of source data were considered for the OEF map generation using a method introduced by the previous article [30] (Fig. 1). It is known that dHb is paramagnetic due to four unpaired electrons of heme, leading to an increase in venous blood susceptibility compared to the surrounding tissue (Fig. 1.b). Our OEF calculation method requires the two factors of vein and tissue to calculate their difference in a volume-of-interest (VOI) since it cannot be obtained by pixel-wise calculations. Hence, in our study, QSM-OEF reflects oxygenation within venous structures, but it might not reflect its value within

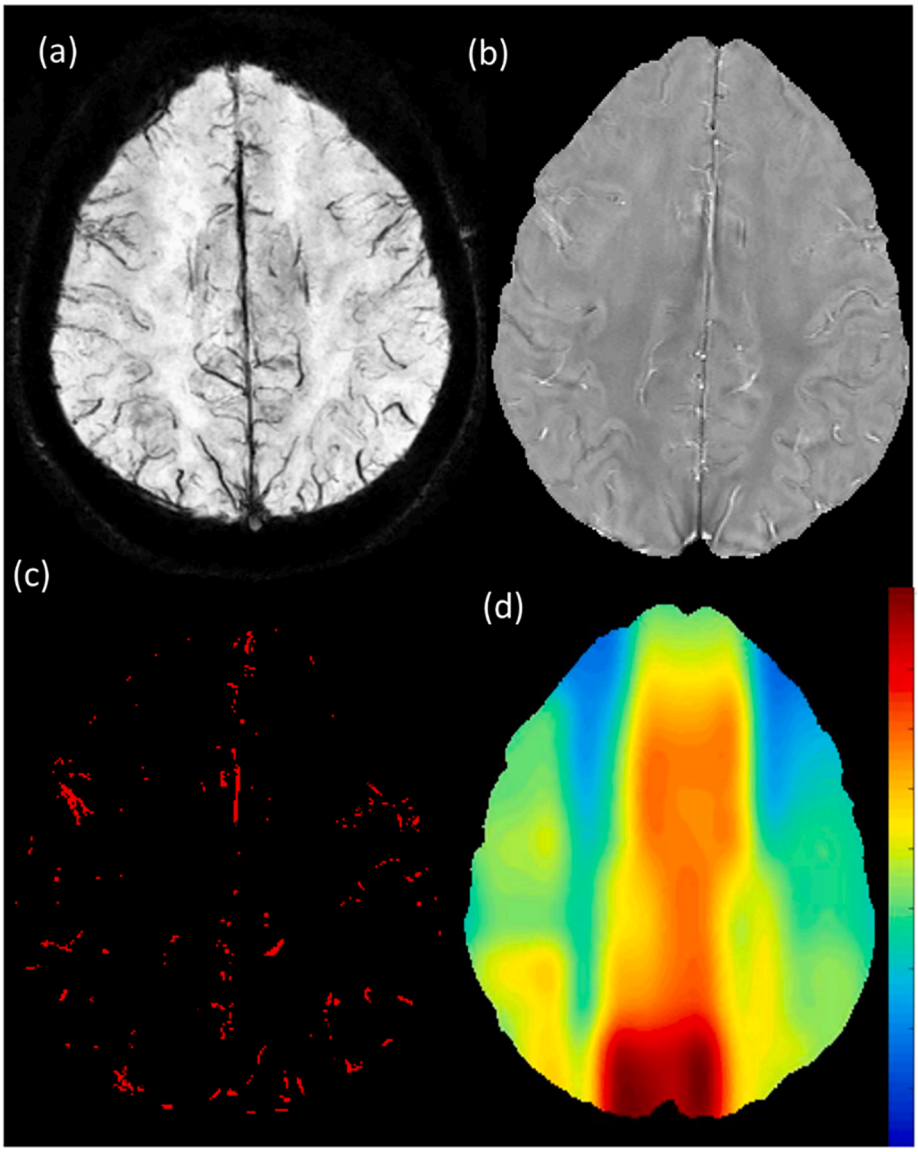

Fig. 1. Creation of Oxygen Extraction Fraction (OEF) map. a) Minimum intensity projection of SWI images [31] for a 37-year-old MRI-negative woman with refractory epilepsy. b) The QSM in which bright pixels indicate the susceptibility of deoxygenated Hb. c) Venous mask obtained from a certain threshold (mean ± 2SD). d) QSM-OEF map generated from the venous mask using the sliding window method. QSM-OEF has been applied Gaussian smoothing filter with kernel size σ = 10.

brain parenchyma like PET-OEF. Therefore, a local threshold value of mean ± 2SD was considered to segment the venous voxels (Fig. 1.c) in each VOI of 64 × 64 × 30 voxels.

Then, susceptibility difference ($\Delta\chi$) between the average susceptibility of veins (vein mask images) and surrounding tissues was calculated in each VOI. The following equation shows the relation between oxygen saturation and susceptibility [20]:

$$\Delta\chi = \Delta\chi_{do} \times Hct \times (1 - Y_v) \times \frac{1}{P_v} \quad (1)$$

where $\Delta\chi_{do}$ (1.8×10^7 in CGS units) is the susceptibility difference per unit hematocrit (Hct) between fully deoxygenated and fully oxygenated blood. OEF is defined as $(Y_a - Y_v)/Y_a$, where Y_a and Y_v are arterial and venous oxygen saturation, respectively. In normal respiratory, Y_a is nearly 100% [32], and thus, the OEF can be defined as $(1 - Y_v)$. According to Eq. (1), OEF is calculated using the following equation:

$$OEF = \frac{\Delta\chi \times P_v}{Hct \times \Delta\chi_{do}} \quad (2)$$

The mean value in each VOI was measured as the mean OEF value of vessels. Subsequently, using the sliding window method in X and Y directions with increments of 10 mm, VOI was applied to whole images, and OEF maps were generated on a slice-by-slice basis (Fig. 1.d). We did not measure the actual amount of hematocrit for each patient due to the low frequency of anemia in seizures. Therefore, we assumed the literature value of 0.42 for Hct. P_v is the partial volume effects correction factor, which has an essential effect on the contrast-to-noise ratio (CNR), depending on the size of the vessels. According to Fig. 3.b in a previous study [22], we calculated the value of approximately 6.0 when a voxel ratio of 1:3 was applied, with a vessel diameter equivalent to 2 pixels.

2.4. Image analysis

Standard Statistical Parameter Mapping (SPM12) software (Welcome Department of Imaging Neuroscience, University College London, UK) (http://www.fil.ion.ucl.ac.uk/spm/software/spm12) was used for linear co-registration of SWI-magnitude to Montreal Neurological Institute (MNI) space using avg152T1.nii image, in which image series were firstly re-landmarked if the image center was far from the origin. The default parameters for all the subjects were similar. The resulting transform matrix was then multiplied to OEF images to bring them into MNI space. Afterward, nonlinear co-registration of OEF maps and standard images was performed employing advanced normalization tools (ANTs) package [33,34].

18 spherical ROIs with a diameter of 10 mm (16 pixels) were drawn using the Marsbar of the SPM12 toolbox. For quantitative measurements, the centers of ROIs were automatically placed on a slice at the level of centrum semiovale of registered OEF images (block-type) along the entire parenchymal surface of the brain, without overlapping each other (Fig. 2) using an image analysis program (ITK-SNAP, www.itksnap.org) [35]. The ROIs' measurement in final QSM-OEF maps (block-type images) was performed before applying Gaussian smoothing.

2.5. Statistical analysis

MATLAB R2019a programming environment was used for performing statistical analyses considering $P < 0.05$ as a significant difference. The REPs were classified into two groups, focal and generalized onset seizure, based on their semiology and LTM findings. We compared the clinical and imaging characteristics between REPs and HS, as well as focal and generalized-onset seizure groups using the two-sample *t*-test.

QSM-OEF values were expressed as the mean ± SD for each of the ROIs. Differences in mean QSM-OEF values of 18 ROIs on the ipsilateral and contralateral sides were compared for REPs and HS, as well as for two patient groups using *t*-test. For generalized-onset patients and HS, the left hemisphere was considered as the ipsilateral side.

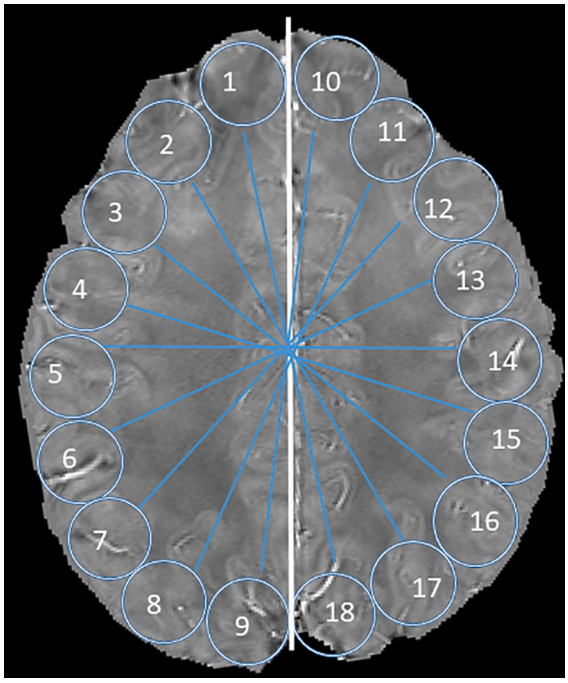

Fig. 2. An example of the regions-of-interest (ROIs) measurement is shown. Using the Marsbar toolbox of the SPM12, 18 spherical ROIs with a 10 mm diameter were automatically drawn and then placed on the entire parenchymal surface of a slice at the level of centrum semioval of the brain.

Pearson's correlation coefficients were calculated to examine correlations between the ipsilateral QSM-OEF changes and the clinical parameters, as well as between each ROI and all the others on both ipsilateral and contralateral sides. The Weibull distribution density function was fitted to investigate the skewness of the mean QSM-OEF values of both sides for REPs and HS.

2.6. Machine learning

Machine learning has become a robust tool in the field of biomedical imaging to perform prediction results based on clinical experimental data. The prediction of the epileptic disease activity having the imaging characteristics of the ROIs was performed using the support vector machine (SVM) algorithm [36–39]. The SVM algorithm uses the training and testing steps in which training means feeding known data to the SVM along with previously known decision values, thus creating a finite training set. Two types of SVM, i.e., C-SVM and η-SVMs are the most conventional prediction methods that can be used for classification problems. C and η parameters in these algorithms should be selected carefully to achieve the best results. Several optimization methods, namely, ant colony optimization (ACO), genetic algorithm (GA), particle swarm optimization (PSO), and differential evolution (DE), were used to optimize the parameters of the machine. The most common criteria to describe the performance of a diagnostic test in measuring the percentage of correctly identified REPs and HS are accuracy (Eq. (3)), sensitivity (Eq. (4)), specificity (Eq. (5)), precision (Eq. (6)), and the area under the curve (AUC).

$$Accuracy = \frac{TP + TN}{TP + TN + FP + FN} \quad (3)$$

$$Sensitivity = \frac{TP}{TP + FN} \quad (4)$$

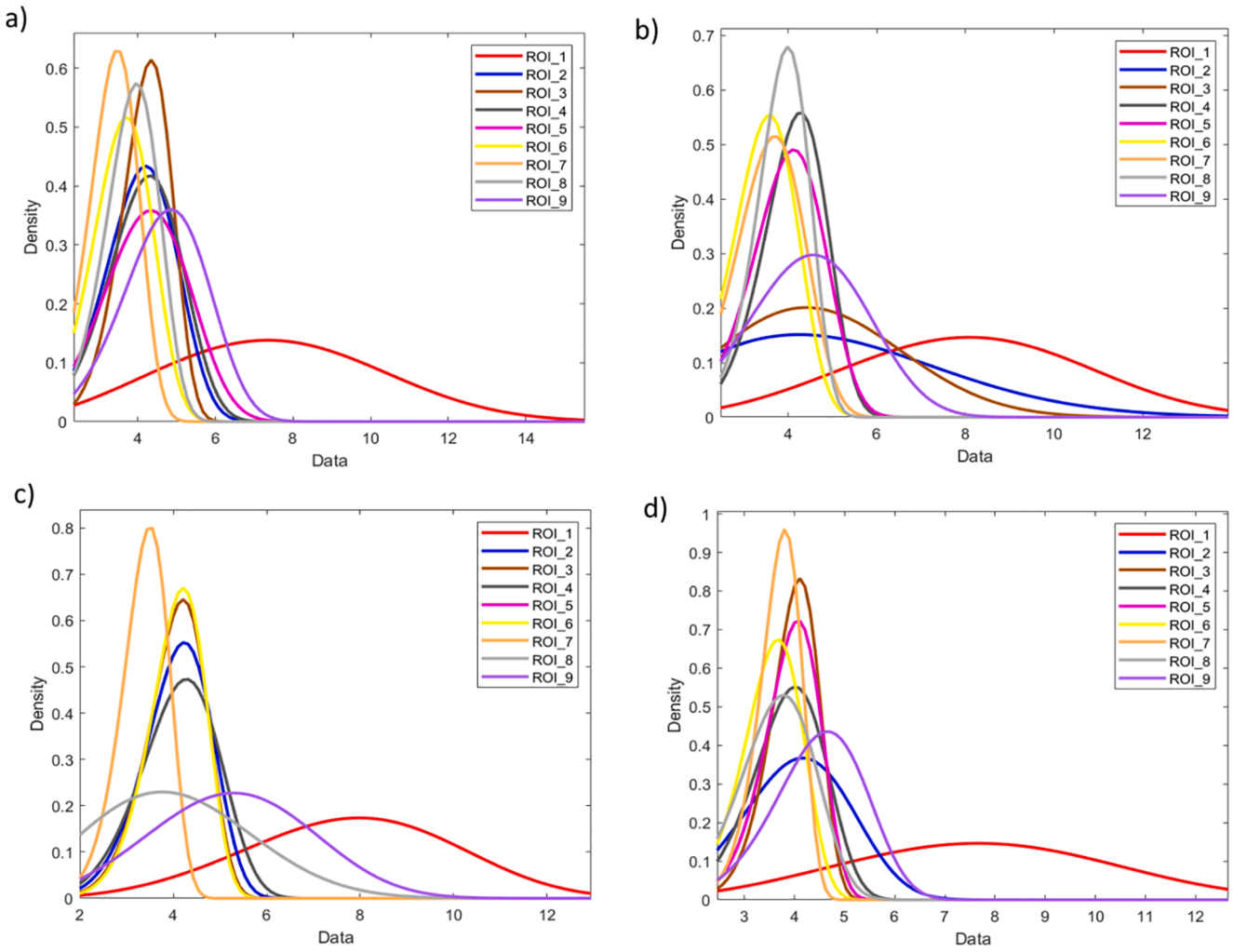

Fig. 3. Weibull distribution curves of mean QSM-OEF in 9 ROIs on the ipsilateral and contralateral sides for REPs (a & b) and HS (c & d), respectively.

Table 2
Comparison of the mean QSM-OEF between REPs and HS.

		REPs (n = 26)	HS (n = 16)	P-value
Sex (female %)		14 (53%)	9 (56%)	0.7
Age (mean ± SD)		29.31 ± 8.86	31.13 ± 8.45	0.5
Age-onset (mean ± SD)		11.58 ± 7.02	–	–
Frequency (mean ± SD)		9.42 ± 14.10	–	–
Duration (mean ± SD)		5.11 ± 4.08	–	–
Type (Focal-onset %)		17 (65%)	–	–
QSM-OEF in both hemispheres (mean ± SD)		44.9 ± 5.8	41.9 ± 6.2	0.04
Ipsilateral QSM-OEF (mean ± SD)	Focal	44.5 ± 6.6	41.8 ± 6.7	0.01
	Generalized	42.7 ± 9.2		≥ 0.1
Contralateral QSM-OEF (mean ± SD)	Focal	46.4 ± 6.8	41.2 ± 5.8	0.02
	Generalized	44.7 ± 7.6		≥ 0.1

For generalized-onset patients and HS, the left hemisphere was considered as the ipsilateral side. OEF: oxygen extraction fraction; QSM: quantitative susceptibility mapping, n = number.

Table 3
Comparison of QSM-OEF changes between the nine ROIs on the ipsilateral and contralateral sides for the REPs.

Type	ROI No.	Ipsilateral QSM-OEF (mean ± SD)	Contralateral QSM-OEF (mean ± SD)	P-value
Focal-onset seizure (n = 17)	1	77.5 ± 12.6	81.5 ± 14.3	0.1
	2	40.1 ± 8.4	50.8 ± 10.1	0.8
	3	42.3 ± 9.9	46.8 ± 6.6	0.9
	4	42.7 ± 9.1	42.3 ± 6.9	**0.005**
	5	42.6 ± 4.3	39.8 ± 9.8	**0.007**
	6	35.0 ± 4.1	35.9 ± 6.3	0.07
	7	34.6 ± 5.9	36.4 ± 7.1	**0.006**
	8	38.6 ± 5.2	38.8 ± 6.5	0.05
	9	45.6 ± 9.7	47.6 ± 10.4	**0.002**
Average		**44.5 ± 6.6**	**46.4 ± 6.8**	
Generalized-onset seizure (n = 9)	1	71.2 ± 12.9	78.6 ± 15.7	0.5
	2	40.4 ± 13.6	53.6 ± 12.0	0.2
	3	40.3 ± 12.0	47.8 ± 13.3	0.3
	4	38.8 ± 4.5	39.4 ± 5.5	0.6
	5	41.4 ± 9.4	40.5 ± 7.5	0.6
	6	35.3 ± 8.7	33.7 ± 7.5	0.4
	7	31.1 ± 5.7	33.9 ± 3.0	0.1
	8	36.9 ± 5.3	36.9 ± 5.7	0.6
	9	48.5 ± 9.0	39.5 ± 6.1	**0.02**
Average		**42.7 ± 9.2**	**44.7 ± 7.6**	

For generalized-onset patients, the left hemisphere was considered as the ipsilateral side. OEF: oxygen extraction fraction; QSM: quantitative susceptibility mapping.

$$Specificity = \frac{TN}{TN + FP} \tag{5}$$

$$Precision = \frac{TP}{TP + FP} \tag{6}$$

where TP is the number of REPs correctly classified, TN is the number of HS correctly classified, FP is the number of HS classified as REPs, and FN is the number of REPs classified as HS.

3. Results

No statistically significant difference was observed in the age and sex for the REPs and HS (P > 0.5). QSM-OEF was significantly higher in REPs (44.9 ± 5.8) than that in HS (41.9 ± 6.2) ($P < 0.05$). Moreover, a statistically significant difference in mean QSM-OEF was observed between focal (45.9 ± 6.2) and generalized (43.7 ± 5.1) onset seizure patients (P < 0.05) (Table 2). In comparison between the ipsilateral and contralateral sides, mean QSM-OEF was significantly lower in the ipsilateral for both the focal-onset (44.5 ± 6.6) (P < 0.01) and generalized-onset (42.7 ± 9.2) (P < 0.05) seizure than that in the contralateral side (46.4 ± 6.8) and (44.7 ± 7.6), respectively (Table 3).

A graphical representation of the distribution of QSM-OEF values in the study of ROIs for both healthy and epileptic subjects can be useful to investigate how QSM-OEF values change for the subjects. Therefore, Weibull distribution curves were fitted to the experimental data to show the differences. Since this type of distribution fitting reveals the skewness of data, it is a proper method for studying the trend of QSM-OEF changes in the ROIs. The distribution curves of nine ROIs of the ipsilateral and contralateral hemisphere to seizure onset for REPs and HS are depicted in Fig. 3.

Pearson's correlation analysis represented that there was a positive correlation between each ROI and the others on the ipsilateral side, as well as between the nine ROIs on both sides for the focal-onset (P ≤ 0.01, $r = 0.6$) (Table 4) and generalized-onset (P < 0.05, $r = 0.6$) (Fig. 4) groups. QSM-OEF had a strong positive correlation with the attack duration (r = 0.6), as well as a moderate negative correlation with the attack frequency (r = −0.3) for focal-onset group (Fig. 5).

Table 5 indicates the performance of the C-SVM and η-SVM machine learning methods in the prediction of the disease in subjects having the

Table 4
Correlation between QSM-OEF changes in ipsilateral and contralateral ROIs across the focal-onset seizures.

	1	2	3	4	5	6	7	8	9	10	11	12	13	14	15	16	17	18
1	1									0.403	−0.372	−0.168	0.241	0.450	0.353	0.066	0.151	0.395
	0									0.1	0.1	0.5	0.3	0.07	0.1	0.8	0.5	0.1
2	0.426	1								−0.117	−0.056	0.082	0.416	0.146	0.324	0.328	0.465	0.433
	0.08	0								0.6	0.8	0.7	0.09	0.5	0.2	0.2	0.06	0.08
3	0.063	0.065	1							0.510	0.104	0.026	**0.663**	**0.610**	0.336	**0.612**	0.510	0.440
	0.8	0.8	0							0.03	0.60	0.9	**0.003**	**0.01**	0.1	**0.009**	0.04	0.07
4	0.196	0.196	**0.861**	1						0.546	0.026	−0.001	**0.750**	**0.680**	0.381	**0.609**	0.463	**0.650**
	0.4	0.4	**0.009**	0						0.02	0.9	0.9	**0.005**	**0.002**	0.1	**0.01**	0.06	**0.007**
5	0.248	−0.028	**0.695**	**0.766**	1					**0.612**	0.166	0.193	**0.692**	**0.735**	0.345	0.504	0.305	0.450
	0.3	0.9	**0.002**	**0.003**	0					**0.01**	0.5	0.4	**0.002**	**0.007**	0.1	0.04	0.2	0.07
6	−0.111	−0.093	0.271	0.360	**0.602**	1				0.196	**0.774**	**0.760**	0.420	0.427	0.454	**0.621**	0.505	0.241
	0.6	0.7	0.3	0.1	**0.01**	0				0.4	**0.002**	**0.003**	0.09	0.08	0.07	**0.01**	0.03	0.3
7	−0.028	0.254	0.369	0.276	0.355	**0.701**	1			0.121	**0.611**	**0.655**	0.417	0.423	**0.611**	**0.637**	**0.761**	0.386
	0.8	0.3	0.1	0.2	0.1	**0.002**	0			0.6	**0.009**	**0.005**	0.09	0.09	**0.01**	**0.006**	**0.001**	0.1
8	0.007	0.053	0.511	0.436	0.455	**0.680**	**0.681**	1		0.423	**0.662**	**0.622**	0.341	**0.671**	**0.803**	**0.638**	**0.607**	0.135
	0.9	0.8	0.03	0.08	0.06	**0.003**	**0.003**	0		0.09	**0.003**	**0.01**	0.1	**0.003**	**0.0001**	**0.005**	**0.01**	0.6
9	**0.614**	0.419	0.501	**0.660**	0.480	0.184	0.227	0.413	1	0.353	−0.072	0.052	**0.638**	**0.617**	0.471	**0.621**	0.455	**0.683**
	0.01	0.09	0.04	**0.003**	0.05	0.4	0.3	0.09	0	0.1	0.7	0.8	**0.005**	**0.01**	0.05	**0.007**	0.04	**0.002**

Pearson's correlation coefficients (r) and significant levels (P) (top and bottom values, respectively) are given. Correlations were calculated between each pair of ipsilateral ROIs, as well as ipsilateral and contralateral ROIs. Regions with significant correlation at the level lower than 0.02 are shown in bold.

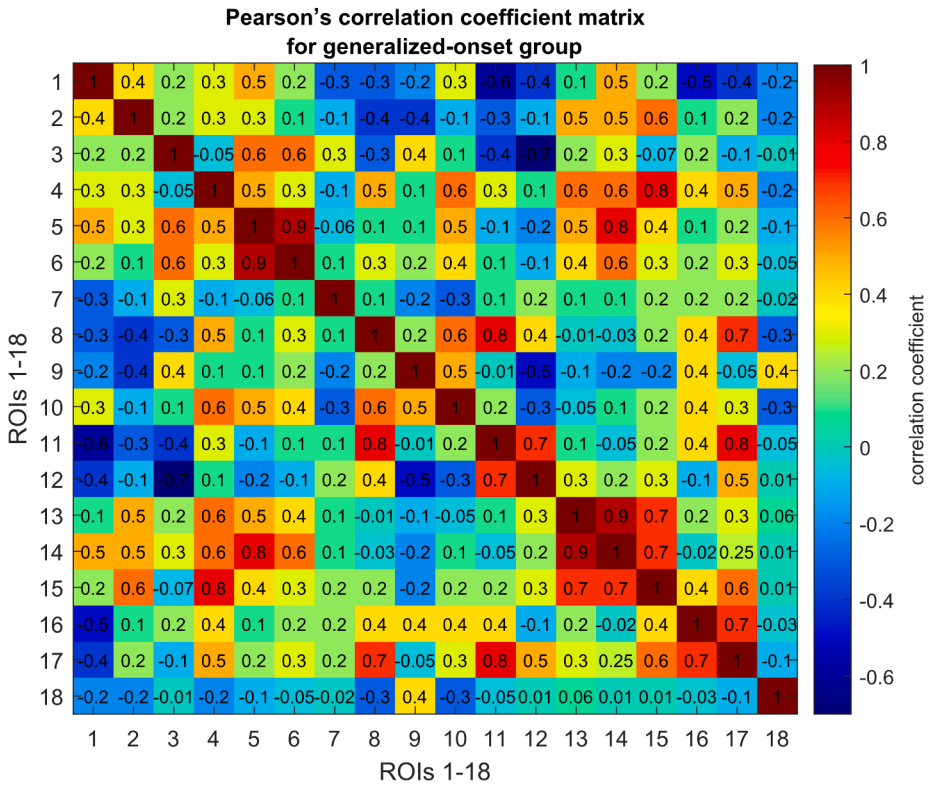

Fig. 4. Pairwise correlation coefficient matrix of 18 ROIs in both hemispheres for the generalized-onset group. There are both significant and moderate correlation between QSM-OEF in corresponding as well as non-corresponding ROIs ($P < 0.05$, $r = 0.6$).

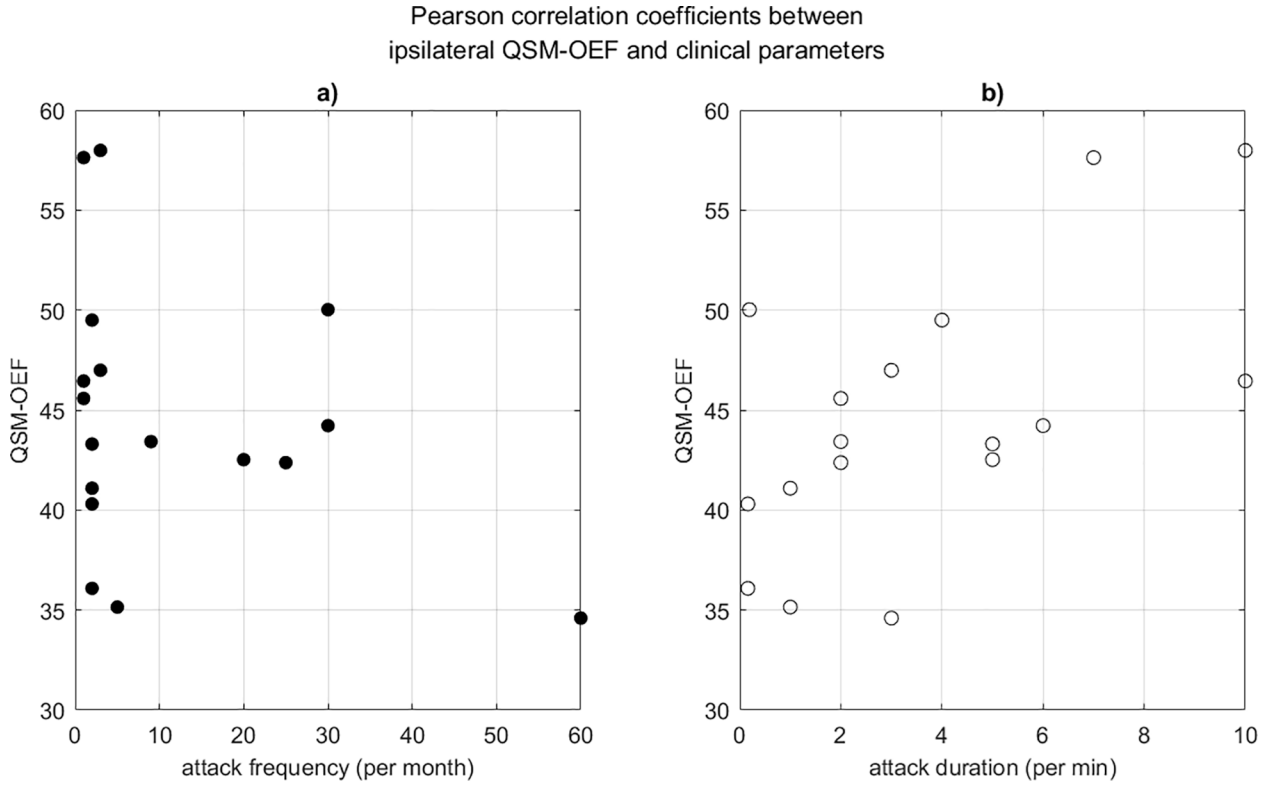

Fig. 5. Scatter plots of Pearson's correlation coefficients between QSM-OEF and two clinical parameters (attack frequency and attack duration) for focal-onset group. QSM-OEF had a moderate negative correlation with the attack frequency ($r = -0.3$) (a), as well as a strong positive correlation with the attack duration ($r = 0.6$) (b).

Table 5
Performance of the C-SVM and η-SVM machine learning methods.

Kernel type	Kernel parameter	Optimization method	Accuracy (C-SVM)	Accuracy (η-SVM)
Linear	0.1	ACO	92.9	92.9
		GA	88.1	92.9
		PSO	88.1	92.9
		DE	92.9	85.7
	0.5	ACO	**97.6**	92.9
		GA	85.7	90.4
		PSO	92.9	88.1
		DE	85.7	85.7
	1	ACO	85.7	88.1
		GA	88.1	**95.2**
		PSO	92.9	90.4
		DE	88.1	92.9
Polynomial	0.1	ACO	**95.2**	**97.6**
		GA	92.9	92.9
		PSO	85.7	85.7
		DE	**95.2**	92.9
	0.5	ACO	**95.2**	**97.6**
		GA	92.9	88.1
		PSO	92.9	92.9
		DE	90.4	**95.2**
	1	ACO	92.9	92.9
		GA	**95.2**	92.9
		PSO	92.9	**95.2**
		DE	92.9	88.1
Gaussian	0.1	ACO	92.9	**97.6**
		GA	**95.2**	88.1
		PSO	92.9	85.7
		DE	**95.2**	85.7
	0.5	ACO	**97.6**	92.9
		GA	**97.6**	**95.2**
		PSO	85.7	92.9
		DE	88.1	90.4
	1	ACO	90.4	**95.2**
		GA	85.7	85.7
		PSO	90.4	**95.2**
		DE	92.9	92.9

SVM: support vector machine; ACO: ant colony optimization; GA: genetic algorithm; PSO: particle swarm optimization; DE: differential evolution. The accuracies of more than 95 are shown in bold.

QSM-OEF data of 18 spherical ROIs. This table indicates the effects of kernel type, parameter type, and optimization method on the accuracy of prediction. A good prediction with accuracy values near 1 can be considered as a useful tool for physicians to reliably detect the status of the subject in the least possible time. This could provide the physicians with valuable information about the subjects and promote the treatment steps. Table 5 presents that overall, the prediction accuracy of SVM is more than 0.9, which indicates that out of 10 subjects, the epilepsy status of at least nine subjects is anticipated correctly using machine learning. By selecting the correct learning type, optimization type, and kernel function, the sensitivity, specificity, AUC, and precision of predicting epileptic and healthy subjects were 0.96, 1, 0.98, and 1, respectively, which revealed the capability of the proposed method in detecting epileptic oxygen metabolism patterns.

4. Discussion

In the current study, we performed an MRI-based study of oxygen metabolism measurement in an intractable epileptic population. Precise QSM-OEF maps of epileptic patients, as well as healthy brain subjects, were obtained using the susceptibility quantification of dHb in veins during interictal states. The relationship between the concentration of dHb in a vein ([dHb]), the CBF, and the cerebral metabolic rate of oxygen are expressed as Eq. (7).

$$CMRO_2 = [dHb] \times CBF \tag{7}$$

On the other hand, the relationship between [dHb] and OEF is:

$$[dHb] = OEF \times O_2 \tag{8}$$

where O_2 is oxygen supply. Substituting Eq. (8) in Eq. (7), it is obtained:

$$CMRO_2 = OEF \times CBF \times O_2 \tag{9}$$

It was shown that OEF at the venule level is directly proportional to the cerebral metabolic rate and inversely proportional to CBF. Absolute quantification of OEF can offer a non-invasive means to investigate brain conditions in REPs. In contrast to the previous justification of CBF and its patterns in the epileptic brain [40–43], the related cerebral oxygen metabolism aspects are still unclear. We compared QSM-OEF between HS and REPs and observed a positive correlation between OEF in the ipsilateral hemisphere and contralateral one in the epileptic group. Since patients were MRI-negative, the ipsilateral sides were determined based on LTM findings. In this study, OEF values were significantly higher in REPs than those in HS, which is consistent with other OEF measurement studies based on PET [44–47]. Elevation of OEF would expect that the epilepsy-associated neuroinflammatory pathways are associated with BBB dysfunction in the brain [48]. The infiltration of peripheral immune cells across the BBB has been described in epilepsy [49–51]. The ipsilateral hemispheres represented an increase in OEF, whereas the contralateral hemispheres compared to the age-matched controls represented an increase as well. These findings could be related to the hypothesis of developing a mirror focus of seizure among epileptic populations. On the other hand, for the REPs' group, sides of seizure onset were associated with significant decreases in QSM-OEF compared with contralateral ones.

Currently, PET is considered the gold standard method for OEF measurement. In contrast with MRI, which is widely available in most clinical centers, OEF measurement by PET is limited, especially for REPs whose seizures are unpredictable. Several significant problems, such as inaccessibility, high costs of PET scanners as well as prohibition to rescan due to using radiation exposure restrict the utility of PET. Therefore, OEF measurement using MRI might be helpful to handle the oxygen metabolism of epileptic patients. By comparing the previous MRI approaches [18,19,52,53] on QSM-based methods, several advantages, such as conventional sequence usage, short acquisition time, being not invasive, and high sensitivity to low perfusion status are reported for the availability of QSM in clinical studies. Nevertheless, this method possesses several disadvantages, make it dependent on the various algorithms [27,29,54,55] for estimating the magnetic susceptibility of substances. Preserving the small veins, which are necessary to calculate accurate OEF values, distinguishes the algorithms for QSM generation. In a 7 T MRI study, Uwano et. al. [23] showed that the QSM-OEF values in chronic ischemia only had a slight improvement in terms of the correlation coefficient and the sensitivity/specificity for PET-OEF compared with those at 3 T reports [30]. Hence, QSM-OEF results obtained from the 3 T scanner can be validated.

The brain energy demand depends on glucose and the supply of oxygen for aerobic metabolism. In a stimulated brain zone, the adenosine triphosphate (ATP) production occurs mainly in the mitochondria of neurons through a phosphorylation process requiring oxygen. This leads to increased $CMRO_2$ and decreased oxygen partial pressure (PO_2). At the same time, some neural and glial mechanisms start to release vasoactive substances [56,57], resulting in a two-fold increment in CBF compared to $CMRO_2$ in the stimulated zone [58]. During minutes of status epilepticus onset, oxygen consumption rates typically increase. However, a predominantly increase in reactive oxygen species [ROS] leads to decreased oxygen consumption after approximately 24 h. Then, it returns to a normal state during the interictal period and decreases during chronic epilepsy, which is termed hypoxia [54]. The frequent seizures cause chronic hypoxia/hypoperfusion that could lead to diminutions in blood flow and metabolism in the epileptogenic zones. It is believed that the epileptic focus is hypoperfused and hypometabolic

during interictal states. Furthermore, structural changes in the brain occur due to frequent seizure activity, and these may also be causally related to interictal comorbidities [59].

To explain the mechanism of incremented OEF in the brain of REPs in this study, we hypothesized that abnormal perfusion, which represents ischemic tissue, may occur. This pathogenesis has been supported by many previous studies that have demonstrated small vessel injury due to vasculitis in epileptic brains [60–62]. The elevation of OEF during interictal state can suggest that there is an imbalance between blood flow and oxygen consumption, which might mean that reserve of oxygen supply in CBF is not enough to provide oxygen metabolic requirements of epileptic brain tissues. The vascular and metabolic decreases are not proportional, which might mean that the hypoperfusion is more than hypometabolism, leading to an increase in OEF in REPs during the interictal state. The contralateral OEF elevation reveals that the area of hypometabolism might be able to extend beyond the epileptogenic zone. According to our study's finding, it seems that one of the noxious aspects of seizures might be vascular incompetency, which leads to hypoperfusion and hypoxia in seizure areas. It could suggest that there is a potential of an imbalance between blood flow and oxygen consumption, which means compared to hypometabolism, hypoperfusion exceeds leading to an increment in OEF in REPs during the interictal state. Therefore, this issue could convince neurologists that there is a relationship between epilepsy and stroke. Vascular incompetency in seizure pathophysiology and behavioral dysfunction can suggest a new strategy of therapy for seizure populations. On the other hand, in the ictal phase, the increase of CBF exceeds the increase of $CMRO_2$, leading to the reduction in OEF. Therefore, a reduction in OEF in the ipsilateral sides compared with contralateral sides, which is concordant with our findings, could be due to the impact of some defects in mitochondria's function, where results in a reduction of oxygen consumption rate in seizure zones [63]. Such findings might raise this question in mind how much hypoxia's intensity can explicate the adverse effects related to seizures during the interictal state. Thus, the lack of an imaging biomarker of disease status and other investigations about seizure-induced vascular related dysfunction, as well as the exploration of potentially novel treatment strategies still remain. These contents show the importance of OEF assessment using non-invasive methods as a clinical application to investigate the severity of disease activity in intractable epileptic patients.

To investigate the ROIs' connectivity, Pearson correlation coefficient measurement was applied to data that has been averaged across voxels within the ROIs. Averaging all the voxels in an ROI and using that in a correlation analysis may often miss correlations because the actual part of the region showing an interesting signal is averaged out. Therefore, it is necessary to take into consideration the resolution of the imaging system versus the size of the ROI in which there is no inhomogeneity within those ROIs. Since in our study, we used nine ROIs in each hemisphere, it was of interest to see if correlations between oxygenation of different sites were presented. A strong positive correlation between several ROIs on the ipsilateral side, as well as between ROIs on the ipsilateral side and the others on the contralateral side was found for both focal-onset (Table 4) and generalized-onset (Fig. 5) seizure groups, demonstrating that changes in these structures tend to occur in the same direction. Perhaps most interestingly, there was no negative correlation between changes in ROIs on both sides. This ROI-based analysis results may suggest that a long-range network effect might have an important metabolic role in refractable epileptic patients.

The utility of machine learning algorithms that exploit brain imaging data has become an interesting and practical topic for neuroimaging studies. A classifier aims to group items that have similar feature values into groups by making a classification decision based on the value of the linear combination of the features. SVM is a robust classification method based on the structural risk minimization that a model takes based on training data to classify new unknown/known data [39]. The usage of SVM in the field of epilepsy has been evaluated in many studies [64–67]. Beheshti et al. [68] used the SVM to assess the proposed lateralization framework in 27 right and 29 left MRI-negative TLE patients to show that pattern analysis of glucose metabolic brain data can lateralize MRI-negative TLE patients in the clinical setting with an accuracy of about 96.43%. Their results were in concordance with an experienced PET interpreter. In another investigation, Cantor-Rivera et al. [69] proposed a method that combined T1 images, quantitative relaxometry, and mean diffusivity with SVM aiming to improve TLE detection. They evaluated various classification models and reported an accuracy of 100% for the nine left-sided seizure onset patients and 88.9% for the eight right-sided seizure onset patients. In the present project, 18 ROIs as features were used for the classification of participants using the machine learning method to evaluate the capability of the QSM-OEF method in realizing that whether a participant is truly sick or not. Due to the poor performance of the artificial neural networks compared to other machine learning methods [70,71], the SVM algorithm was considered. Preliminary results of the SVM calculation had an accuracy of about 60%, which was not favorable. To avoid adjusting the SVM's parameters manually, we used four advanced optimization methods to improve the performance of the machine. Using these optimization methods, the accuracy of the results increased up to 97%. That is, out of every 42 samples, only one sample was incorrectly classified. Therefore, using the SVM method and 18 features (18 ROIs), we were able to determine if a person suffers from epilepsy with an accuracy of more than 95% (Table 5).

This study faced several limitations that should be considered to explicate consequences. The most notable limitation was the lack of CBF measurement for patients to investigate the relationships between OEF and $CMRO_2$ in epileptic brains since the concentration of dHb in venous is proportional to the $CMRO_2$ and inverse proportional to the CBF. The lack of measuring Hct and or Hb in patients was another deficiency as the decay of the blood's T1 signal depends greatly on the level of Hct. If the Hct is high, the blood's T1 signal decays rapidly, and CBF is less than normal. However, if the Hct is low, the blood's T1 signal decays very slowly, and the CBF is higher than normal [72]. Additionally, it was necessary to include only slices above the basal ganglia, in which the existence of iron can adversely affect the susceptibility of voxels include the dHb. The low spatial resolution of OEF maps due to keeping the homogeneity was another drawback. This required the number of venous voxels not to be too low. On the other hand, the spatial resolution in OEF images depends on the size of VOI. So, there was a trade-off between a higher spatial resolution and the homogeneity of OEF maps. We hope future investigations create more advanced venous masks to overcome this limitation. Besides, although a correction factor for partial volume effects was applied in this study, it is necessary to improve the quantification of cerebral oxygenation by this factor in each vessel separately [73]. The number of subjects was also limited since most of the patients recruited to our hospital had received anti-epileptic drugs and had brain surgery before MR imaging, whose data was not useable in this work. Finally, measuring OEF was limited only to spherical ROIs centered on a two-dimensional slice. Applying standard three-dimensional ROIs [24] might result in more accurate and reliable outcomes.

5. Conclusion

The QSM method is a feasible technique to create an OEF map. The results of this study revealed that QSM-OEF of the REPs' brain is higher than that of HS, which indicates that QSM-OEF is associated with disease activity. The OEF elevation represents the reactive changes of the small vessels that may occur as a result of the neuroinflammatory activity. This consequence offers new insights into the characterization of hemodynamic deficiency and physiology of the refractory epileptic brain. An increment in OEF may provide an opportunity to convince the medical community that epilepsy is not only an electrical disorder but could also be a vascular-based (physiological and metabolic) disorder.

This means that hypoxic attacks could result in seizures. Seizures initiate a cascade of events that result in vasoconstriction, leading to hypoperfusion/hypoxia with its own set of neurologic consequences.

Acknowledgments

This study was funded and supported by Tehran University of Medical Sciences (TUMS); Grant no: 96-04-30-36970. The authors thank the Epilepsy clinic of Imam Khomeini Hospital, Tehran, Iran, to assort the patients and also the National Brain Mapping Lab, Tehran, Iran, for imaging data acquisition. The authors acknowledge Dr. Ikuko Uwano from Iwate Japan, for generously sharing some helpful information about the QSM-OEF method in this study, as well as Dr. Morteza Najibi from Shiraz University for effective comments in statistical analysis. The authors also acknowledge Dr. Brian B. Avants from the University of Pennsylvania for help with ANTs software implementation.

Declaration of Competing Interest

Conflict of Interests: No conflict of interest was declared.

Ethical approval

Ethics Code: IR.TUMS.MEDICINE.REC.1397.008.

References

[1] England MJ, Liverman CT, Schultz AM, Strawbridge LM. Epilepsy across the spectrum: promoting health and understanding. A summary of the Institute of Medicine report. Epilepsy Behav 2012;25:266–76. https://doi.org/10.1016/j.yebeh.2012.06.016.

[2] Thurman DJ, Begley CE, Carpio A, Helmers S, Hesdorffer DC, Mu J, et al. The primary prevention of epilepsy: a report of the Prevention Task Force of the International League Against Epilepsy. Epilepsia 2018;59:905–14. https://doi.org/10.1111/epi.14068.

[3] Berg AT, Berkovic SF, Brodie MJ, Buchhalter J, Cross JH, Van Emde BW, et al. Revised terminology and concepts for organization of seizures and epilepsies: Report of the ILAE Commission on Classification and Terminology, 2005–2009. Epilepsia 2010;51:676–85. https://doi.org/10.1111/j.1528-1167.2010.02522.x.

[4] Kim T, Nguyen P, Pham N, Bui N, Truong H, Ha S, et al. Epileptic seizure detection and experimental treatment: a review. Front Neurol 2020;11. https://doi.org/10.3389/fneur.2020.00701.

[5] Vikram DS, Zweier JL, Kuppusamy P. Methods for noninvasive imaging of tissue hypoxia. Antioxid Redox Signal 2007;9:1745–56. https://doi.org/10.1089/ars.2007.1717.

[6] Bernal B, Guillen MR, Valdes P, Jayakar P, Altman N, Duchowny M, et al. Epilepsy focus localization in patients utilizing BOLD differences related to regional metabolic dynamics. Open J Radiol 2019;09:163–75. https://doi.org/10.4236/ojrad.2019.93015.

[7] Wei Y, Ullah G, Ingram J, Schiff SJ. Oxygen and seizure dynamics: II. Computational modeling. J Neurophysiol 2014;112:213–23. https://doi.org/10.1152/jn.00541.2013.

[8] Zhang C, Bélanger S, Pouliot P, Lesage F. Measurement of local partial pressure of oxygen in the brain tissue under normoxia and epilepsy with phosphorescence lifetime microscopy. PLoS One 2015;10:1–14. https://doi.org/10.1371/journal.pone.0135536.

[9] Farrell JS, Gaxiola-Valdez I, Wolff MD, David LS, Dika HI, Geeraert BL, et al. Postictal behavioural impairments are due to a severe prolonged hypoperfusion/hypoxia event that is COX-2 dependent. ELife 2016;5:1–24. https://doi.org/10.7554/eLife.19352.

[10] Jiang BH, Semenza GL, Bauer C, Marti HH. Hypoxia-inducible factor 1 levels vary exponentially over a physiologically relevant range of O2 tension. Am J Physiol - Cell Physiol 1996;271:C1172–80. https://doi.org/10.1152/ajpcell.1996.271.4.c1172.

[11] Baron JC, Bousser MG, Rey A, Guillard A, Comar D, Castaigne P. Reversal of focal "misery-perfusion syndrome" by extra-intracranial arterial bypass in hemodynamic cerebral ischemia a case study with18o positron emission tomography. Stroke 1981;12:454–9. https://doi.org/10.1161/01.STR.12.4.454.

[12] Yamauchi H, Higashi T, Kagawa S, Nishii R, Kudo T, Sugimoto K, et al. Is misery perfusion still a predictor of stroke in symptomatic major cerebral artery disease? Brain 2012;135:2515–26. https://doi.org/10.1093/brain/aws131.

[13] Van Vliet EA, Araújo SDC, Redeker S, Van Schaik R, Aronica E, Gorter JA. Blood-brain barrier leakage may lead to progression of temporal lobe epilepsy. Brain 2007;130:521–34. https://doi.org/10.1093/brain/awl318.

[14] Rigau V, Morin M, Rousset MC, De Bock F, Lebrun A, Coubes P, et al. Angiogenesis is associated with blood-brain barrier permeability in temporal lobe epilepsy. Brain 2007;130:1942–56. https://doi.org/10.1093/brain/awm118.

[15] Vezzani A, French J. The role of inflammation in epilepsy. Nature Rev Neuro Rev Neuro 2011;7:31–40. https://doi.org/10.1038/nrneurol.2010.178.

[16] Novy J, Belluzzo M, Caboclo LO, Catarino CB, Yogarajah M, Martinian L, et al. The lifelong course of chronic epilepsy: the Chalfont experience. Brain 2013;136:3187–99. https://doi.org/10.1093/brain/awt117.

[17] Zhu X-H, Chen J. Simultaneous and noninvasive imaging of cerebral oxygen metabolic rate, blood flow and oxygen extraction fraction in stroke mice. NeuroImage 2013;64:437–47. https://doi.org/10.1016/j.neuroimage.2012.09.028.

[18] He X, Yablonskiy DA. Quantitative BOLD: mapping of human cerebral deoxygenated blood volume and oxygen extraction fraction: default state. Magn Reson Med 2007;57:115–26. https://doi.org/10.1002/mrm.21108.

[19] Lu H, Ge Y. Quantitative evaluation of oxygenation in venous vessels using T2-relaxation-under-spin-tagging MRI. Magn Reson Med 2008;60:357–63. https://doi.org/10.1002/mrm.21627.

[20] Zaitsu Y, Kudo K, Terae S, Yazu R, Ishizaka K, Fujima N, et al. Mapping of cerebral oxygen extraction fraction changes with susceptibility-weighted phase imaging. Radiology 2011;261:930–6. https://doi.org/10.1148/radiol.11102416.

[21] Haacke EM, Liu S, Buch S, Zheng W, Wu D, Ye Y. Quantitative susceptibility mapping: current status and future directions. Magn Reson Imaging 2015;33:1–25. https://doi.org/10.1016/j.mri.2014.09.004.

[22] Haacke EM, Tang J, Neelavalli J, Cheng YCN. Susceptibility mapping as a means to visualize veins and quantify oxygen saturation. J Magn Reson Imaging 2010;32:663–76. https://doi.org/10.1002/jmri.22276.

[23] Uwano I, Kudo K, Sato R, Ogasawara K, Kameda H, Nomura JI, et al. Noninvasive assessment of oxygen extraction fraction in chronic ischemia using quantitative susceptibility mapping at 7 Tesla. Stroke 2017;48:2136–41. https://doi.org/10.1161/STROKEAHA.117.017166.

[24] Nomura JI, Uwano I, Sasaki M, Kudo K, Yamashita F, Ito K, et al. Preoperative cerebral oxygen extraction fraction imaging generated from 7t MR quantitative susceptibility mapping predicts development of cerebral hyperperfusion following carotid endarterectomy. Am J Neuroradiol 2017;38:2327–33. https://doi.org/10.3174/ajnr.A5390.

[25] Miyata M, Kakeda S, Kudo K, Iwata S, Tanaka Y, Wang Y, et al. Evaluation of oxygen extraction fraction in systemic lupus erythematosus patients using quantitative susceptibility mapping. J Cereb Blood Flow Metab 2019;39:1648–58. https://doi.org/10.1177/0271678X18764829.

[26] Kwan P, Arzimanoglou A, Berg AT, Brodie MJ, Hauser WA, Mathern G, et al. Definition of drug resistant epilepsy: consensus proposal by the ad hoc Task Force of the ILAE commission on therapeutic strategies. Epilepsia 2010;51:1069–77. https://doi.org/10.1111/j.1528-1167.2009.02397.x.

[27] Schweser F, Deistung A, Reichenbach JR. Foundations of MRI phase imaging and processing for Quantitative Susceptibility Mapping (QSM). Z Med Phys 2016;26:6–34. https://doi.org/10.1016/j.zemedi.2015.10.002.

[28] Li W, Avram A. Integrated Laplacian-based phase unwrapping and background phase removal for quantitative susceptibility mapping. NMR Biomed 2015;27:219–27. https://doi.org/10.1002/nbm.3056.Integrated.

[29] Wu B, Li W, Guidon A, Liu C. Whole brain susceptibility mapping using compressed sensing. Magn Reson Med 2012;67:137–47. https://doi.org/10.1002/mrm.23000.

[30] Kudo K, Liu T, Murakami T, Goodwin J, Uwano I, Yamashita F, et al. Oxygen extraction fraction measurement using quantitative susceptibility mapping : comparison with positron emission tomography 2015. DOI:10.1177/0271678X15606713.

[31] Tang J, Liu S, Neelavalli J, Cheng YCN, Buch S, Haacke EM. Improving susceptibility mapping using a threshold-based K-space/image domain iterative reconstruction approach. Magn Reson Med 2013;69:1396–407. https://doi.org/10.1002/mrm.24384.

[32] Van Zijl PCM, Eleff SM, Ulatowski JA, Oja JME, Uluğ AM, Traystman RJ, et al. Quantitative assessment of blood flow, blood volume and blood oxygenation effects in functional magnetic resonance imaging. Nat Med 1998;4:159–67. https://doi.org/10.1038/nm0298-159.

[33] Avants BB, Yushkevich P, Pluta J, Minkoff D, Korczykowski M, Detre J, et al. The optimal template effect in hippocampus studies of diseased populations. NeuroImage 2010;49:2457–66. https://doi.org/10.1016/j.neuroimage.2009.09.062.

[34] Avants BB, Tustison NJ, Song G, Cook PA, Klein A, Gee JC. A reproducible evaluation of ANTs similarity metric performance in brain image registration. NeuroImage 2011;54:2033–44. https://doi.org/10.1016/j.neuroimage.2010.09.025.

[35] Yushkevich PA, Piven J, Hazlett HC, Smith RG, Ho S, Gee JC, et al. User-guided 3D active contour segmentation of anatomical structures: significantly improved efficiency and reliability. NeuroImage 2006;31:1116–28. https://doi.org/10.1016/j.neuroimage.2006.01.015.

[36] Mourão-Miranda J, Bokde ALW, Born C, Hampel H, Stetter M. Classifying brain states and determining the discriminating activation patterns: Support Vector Machine on functional MRI data. NeuroImage 2005;28:980–95. https://doi.org/10.1016/j.neuroimage.2005.06.070.

[37] Klöppel S, Stonnington CM, Chu C, Draganski B, Scahill RI, Rohrer JD, et al. Automatic classification of MR scans in Alzheimer's disease. Brain 2008;131:681–9. https://doi.org/10.1093/brain/awm319.

[38] Craddock RC, Holtzheimer PE, Hu XP, Mayberg HS. Disease state prediction from resting state functional connectivity. Magn Reson Med 2009;62:1619–28. https://doi.org/10.1002/mrm.22159.

[39] Vapnik VN. An overview of statistical learning theory. IEEE Trans Neural Networks 1999;10:988–99. https://doi.org/10.1109/72.788640.

[40] Gaxiola-Valdez I, Singh S, Perera T, Sandy S, Li E, Federico P. Seizure onset zone localization using postictal hypoperfusion detected by arterial spin labelling MRI. Brain 2017;140:2895–911. https://doi.org/10.1093/brain/awx241.
[41] Liu HL, Kochunov P, Hou J, Pu Y, Mahankali S, Feng CM, et al. Perfusion-weighted imaging of interictal hypoperfusion in temporal lobe epilepsy using FAIR-HASTE: comparison with H215O PET measurements. Magn Reson Med 2001;45:431–5. https://doi.org/10.1002/1522-2594(200103)45:3<431::AID-MRM1056>3.0.CO;2-E.
[42] Placidi F, Floris R, Bozzao A, Romigi A, Tombini M, Baviera ME, et al. Dynamic susceptibility contrast (DSC) MRI and interictal epileptiform activity in cryptogenic partial epilepsy. Epilepsia 2002;43:1515–21. https://doi.org/10.1046/j.1528-1157.2002.04702.x.
[43] Valmier J, Touchon J, Baldy-Moulinier M. Interictal regional cerebral blood flow during non specific activation test in partial epilepsy. J Neurol Neurosurg Psychiatry 1989;52:364–71. https://doi.org/10.1136/jnnp.52.3.364.
[44] Bernardi S, Trimble MR, Frackowiak RSJ, Wise RJ, Jones T. An interictal study of partial epilepsy using positron emission tomography and the oxygen - 15 inhalation technique. J Neurol Neurosurg Psychiatry 1983;46:473–7. https://doi.org/10.1136/jnnp.46.6.473.
[45] Franck G, Sadzot B, Salmon E, Depresseux JC, Grisar T, Peters JM, et al. Regional cerebral blood flow and metabolic rates in human focal epilepsy and status epilepticus. Adv Neurol 1986;44:935–48.
[46] Decoo D, Destée A. PET studies in epilepsy. Acta Neurol Belg 1997;97:196–9.
[47] Gallhofer B, Trimble MR, Frackowiak R, Gibbs J, Jones T. A study of cerebral blood flow and metabolism in epileptic psychosis using positron emission tomography and oxygen. J Neurol Neurosurg Psychiatry 1985;48:201–6. https://doi.org/10.1136/jnnp.48.3.201.
[48] Vezzani A, Friedman A. Brain inflammation as a biomarker in epilepsy. Biomarkers Med 2011;5:607–14. https://doi.org/10.2217/bmm.11.61.
[49] Bauer J, Becker AJ, Elyaman W, Peltola J, Rüegg S, Titulaer MJ, et al. Innate and adaptive immunity in human epilepsies. Epilepsia 2017;58:57–68. https://doi.org/10.1111/epi.13784.
[50] Choi J, Koh S. Role of brain inflammation in epileptogenesis. Yonsei Med J 2008;49:1–18. https://doi.org/10.3349/ymj.2008.49.1.1.
[51] Iyer A, Zurolo E, Spliet WGM, Van Rijen PC, Baayen JC, Gorter JA, et al. Evaluation of the innate and adaptive immunity in type i and type II focal cortical dysplasias. Epilepsia 2010;51:1763–73. https://doi.org/10.1111/j.1528-1167.2010.02547.x.
[52] Bolar DS, Rosen BR, Sorensen AG, Adalsteinsson E. QUantitative Imaging of eXtraction of oxygen and TIssue consumption (QUIXOTIC) using venular-targeted velocity-selective spin labeling. Magn Reson Med 2011;66:1550–62. https://doi.org/10.1002/mrm.22946.
[53] Fan AP, Benner T, Bolar DS, Rosen BR, Adalsteinsson E. Phase-based regional oxygen metabolism (PROM) using MRI. Magn Reson Med 2012;67:669–78. https://doi.org/10.1002/mrm.23050.
[54] Liu T, Liu J, De Rochefort L, Spincemaille P, Khalidov I, Ledoux JR, et al. Morphology enabled dipole inversion (MEDI) from a single-angle acquisition: comparison with COSMOS in human brain imaging. Magn Reson Med 2011;66:777–83. https://doi.org/10.1002/mrm.22816.
[55] Sato R, Shirai T, Taniguchi Y, Murase T, Bito Y, Ochi H. Quantitative susceptibility mapping using the multiple dipole-inversion combination with k-space segmentation method. Magn Resonance Medical Sci 2017;16:340–50. https://doi.org/10.2463/mrms.mp.2016-0062.
[56] Erecinska M, Silver IA. ATP and brain function. J Cereb Blood Flow Metab 1989;9:2–19. https://doi.org/10.1038/jcbfm.1989.2.
[57] Logothetis NK, Pfeuffer J. On the nature of the BOLD fMRI contrast mechanism. Magn Reson Imaging 2004;22:1517–31. https://doi.org/10.1016/j.mri.2004.10.018.
[58] Buxton RB. Interpreting oxygenation-based neuroimaging signals: the importance and the challenge of understanding brain oxygen metabolism. Front Neuroenerg 2010;2:1–16. https://doi.org/10.3389/fnene.2010.00008.
[59] Kleen JK, Scott RC, Holmes GL, Lenck-Santini PP. Cognitive and behavioral comorbidities of epilepsy. vol. 51. 4th editio. 2010. DOI:10.1111/j.1528-1167.2010.02865.x.
[60] Atkinson M, Atkinson B, Norris G, Shah A. Refractory status epilepticus secondary to CNS vasculitis, a role for epilepsy surgery. J Neurol Sci 2012;315:156–9. https://doi.org/10.1016/j.jns.2011.11.029.
[61] Chiu M, Datta A. Childhood small vessel primary angiitis of the central nervous system: a treatable cause of super-refractory status epilepticus. J Child Neurol 2020;35:31–6. https://doi.org/10.1177/0883073819872579.
[62] Goerres GW, Revesz T, Duncan J, Banati RB. Imaging cerebral vasculitis in refractory epilepsy using [11C](R)-PK11195 positron emission tomography. vol. 176. 2001. DOI:10.2214/ajr.176.4.1761016.
[63] Rowley S, Liang LP, Fulton R, Shimizu T, Day B, Patel M. Mitochondrial respiration deficits driven by reactive oxygen species in experimental temporal lobe epilepsy. Neurobiol Dis 2015;75:151–8. https://doi.org/10.1016/j.nbd.2014.12.025.
[64] Keihaninejad S, Heckemann RA, Gousias IS, Hajnal JV, Duncan JS, Aljabar P, et al. Classification and lateralization of temporal lobe epilepsies with and without hippocampal atrophy based on whole-brain automatic mri segmentation. PLoS One 2012;7:1–12. https://doi.org/10.1371/journal.pone.0033096.
[65] Raghu S, Sriraam N, Vasudeva Rao S, Hegde AS, Kubben PL. Automated detection of epileptic seizures using successive decomposition index and support vector machine classifier in long-term EEG. Neural Comput Appl 2020;32:8965–84. https://doi.org/10.1007/s00521-019-04389-1.
[66] Zhang J hui, Han X, Zhao H wei, Zhao D, Wang N, Zhao T, et al. Personalized prediction model for seizure-free epilepsy with levetiracetam therapy: a retrospective data analysis using support vector machine. British Journal of Clinical Pharmacology 2018;84:2615–24. DOI:10.1111/bcp.13720.
[67] Zavar M, Rahati S, Akbarzadeh-T MR, Ghasemifard H. Evolutionary model selection in a wavelet-based support vector machine for automated seizure detection. Expert Syst Appl 2011;38:10751–8. https://doi.org/10.1016/j.eswa.2011.01.087.
[68] Beheshti I, Sone D, Maikusa N, Kimura Y, Shigemoto Y, Sato N, et al. Pattern analysis of glucose metabolic brain data for lateralization of MRI-negative temporal lobe epilepsy. Epilepsy Res 2020;167:106474. https://doi.org/10.1016/j.eplepsyres.2020.106474.
[69] Cantor-Rivera D, Khan AR, Goubran M, Mirsattari SM, Peters TM. Detection of temporal lobe epilepsy using support vector machines in multi-parametric quantitative MR imaging. Comput Med Imaging Graph 2015;41:14–28. https://doi.org/10.1016/j.compmedimag.2014.07.002.
[70] Asefpour Vakilian K. Machine learning improves our knowledge about miRNA functions towards plant abiotic stresses. Sci Rep 2020;10:1–10. https://doi.org/10.1038/s41598-020-59981-6.
[71] Sarlaki E, Sharif Paghaleh A, Kianmehr MH, Asefpour Vakilian K. Valorization of lignite wastes into humic acids: Process optimization, energy efficiency and structural features analysis. Renewable Energy 2021;163:105–22. https://doi.org/10.1016/j.renene.2020.08.096.
[72] Vaclavu L, Van Der Land V, Heijtel DFR, Van Osch MJP, Cnossen MH, Majoie CBLM, et al. In vivo T1 of blood measurements in children with sickle cell disease improve cerebral blood flow quantification from arterial spin-labeling MRI. Am J Neuroradiol 2016;37:1727–32. https://doi.org/10.3174/ajnr.A4793.
[73] Ward PGD, Fan AP, Raniga P, Barnes DG, Dowe DL, Ng ACL, et al. Improved quantification of cerebral vein oxygenation using partial volume correction. Front Neurosci 2017;11:1–12. https://doi.org/10.3389/fnins.2017.00089.